Engineering 4 (2018) 343–351

Contents lists available at ScienceDirect

Engineering

journal homepage: www.elsevier.com/locate/eng

Research
Green Industrial Processes—Review

New Insight into the Development of Oxygen Carrier Materials for Chemical Looping Systems

Zhuo Cheng [a,#], Lang Qin [a,#], Jonathan A. Fan [b], Liang-Shih Fan [a,*]

[a] William G. Lowrie Department of Chemical and Biomolecular Engineering, The Ohio State University, Columbus, OH 43210, USA
[b] Department of Electrical Engineering, Ginzton Laboratory, Stanford University, Stanford, CA 94305, USA

ARTICLE INFO

Article history:
Received 13 December 2017
Revised 20 January 2018
Accepted 7 May 2018
Available online 19 May 2018

Keywords:
Chemical looping
Oxygen carrier
Hydrocarbon conversion
Ionic diffusion
Mechanism

ABSTRACT

Chemical looping combustion (CLC) and chemical looping reforming (CLR) are innovative technologies for clean and efficient hydrocarbon conversion into power, fuels, and chemicals through cyclic redox reactions. Metal oxide materials play an essential role in the chemical looping redox processes. During reduction, the oxygen carriers donate the required amount of oxygen ions for hydrocarbon conversion and product synthesis. In the oxidation step, the depleted metal oxide oxygen carriers are replenished with molecular oxygen from the air while heat is released. In recent years, there have been significant advances in oxygen carrier materials for various chemical looping applications. Among these metal oxide materials, iron-based oxygen carriers are attractive due to their high oxygen-carrying capacity, cost benefits, and versatility in applications for chemical looping reactions. Their reactivity can also be enhanced via structural design and modification. This review discusses recent advances in the development of oxygen carrier materials and the mechanisms of hydrocarbon conversion over these materials. These advances will facilitate the development of oxygen carrier materials for more efficient chemical looping technology applications.

1. Introduction

Cyclic redox reactions of metal oxides are the key to many energy-conversion systems such as photocatalysis and chemical looping [1]. Consequently, improvements in the redox reactivity of metal oxides, made possible by a deep understanding of the associated reaction mechanisms, are critical in energy-related fields. Chemical looping technology has been demonstrated to be one of the most promising and versatile technologies in the clean energy industry. In a chemical looping oxygen uncoupling (CLOU) system, oxygen gas molecules are released through the creation of an oxygen vacancy (V_O):

$$O_O^X \leftrightarrow \frac{1}{2}O_2 + V_O^{\cdot\cdot} + 2e^-$$

where O_O^X denotes the lattice oxygen of metal oxide *X*.

During a regeneration step, the oxygen vacancy is annihilated through the adsorption, dissociation, and diffusion of molecular oxygen (O_2):

$$\frac{1}{2}O_2 + V_O^{\cdot\cdot} \leftrightarrow O_O^X + 2h^+$$

Active oxygen carriers for CLOU applications include transition metal oxides such as copper/manganese-based oxides [2] and modified perovskite materials [3,4]. In a chemical looping combustion (CLC), chemical looping gasification (CLG), or chemical looping reforming (CLR) system, oxygen carriers react with solid or gaseous fuels by providing lattice oxygen in a reducer and are regenerated by air in an oxidizer where heat is released, thus allowing for autothermal operation. Unlike in the CLOU system, lattice oxygen directly reacts with hydrocarbon intermediates in the CLC, CLG, or CLR system without gaseous oxygen being involved in the reducer. According to the carbonaceous feedstock reaction conditions in the reducer, chemical looping reactions can be classified into complete/full oxidation and partial/selective oxidation. Complete/full oxidation represents typical CLC applications, whereas partial/selective oxidation represents CLG or CLR applications. Chemical looping reactions can also be applied to systems without fossil feedstock, such as solar or nuclear systems. Fig. 1 shows four typical chemical looping systems, in which Fig. 1(a) and (b) show the systems with iron(III) oxide (Fe_2O_3) as the oxygen carrier and methane (CH_4) as the carbonaceous feedstock.

* Corresponding author.
E-mail address: fan.1@osu.edu (L.-S. Fan).
The authors contribute equally.

https://doi.org/10.1016/j.eng.2018.05.002

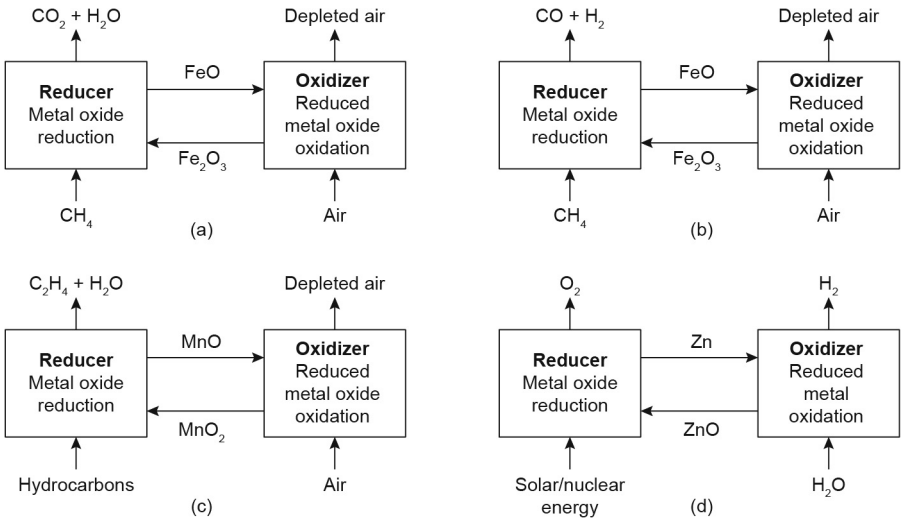

Fig. 1. Classification of chemical looping systems. (a) Complete/full oxidation system; (b) partial oxidation system; (c) selective oxidation system; (d) solar/nuclear system.

Major efforts have been made toward the conversion of various carbonaceous fuels including coal, methane, and biomass to carbon monoxide and hydrogen with improved utilization efficiency based on the chemical looping concept [5]. Nevertheless, the design and improvement of cost-effective, environmentally friendly, highly reactive, and recyclable oxygen carrier materials remain a challenging topic due to the complex reaction mechanism in chemical looping redox reactions. Extensive research has been conducted into the development of optimum oxygen carrier materials. During the early stages of development, these studies focused on single-component materials. More recently, the development of oxygen carriers has been directed toward using multiple metal-based composite materials for performance enhancement, such as binary metals or bimetallic oxygen carriers [6]. Different with the conversion reactions of carbonaceous fuels on solid catalysts which have stable reaction structures, the cyclic chemical looping reactions are accompanied by a tremendous change in the morphology of solid oxygen carriers due to the ionic diffusion and oxygen vacancy formation both in the bulk and on the surface of the oxygen carriers. With the development of advanced experimental techniques, computation, and simulation, the field of chemical looping has attracted increasing attention in the past decade. In this article, we focus on new insight into the development of oxygen carriers for chemical looping systems based on the latest theoretical and experimental studies.

2. Ionic diffusion with morphological evolution

The morphological evolution of oxygen carriers plays a significant role in chemical looping processes because it determines the reaction surface area and structural stability. During redox reactions, the morphology evolves with the ionic diffusion in the solid phase. Therefore, an understanding of ionic diffusion is crucial in the development of oxygen carriers.

To determine the ionic diffusion mechanism macroscopically, inert marker experiments have been performed on many oxygen carrier materials. Li et al. [7] studied the effect of titanium dioxide (TiO_2) support in Fe_2O_3 during oxidation, and found that the dominating ionic-transfer mechanism changes from the outward diffusion of iron (Fe) ions to the inward diffusion of oxygen (O) ions. Naturally occurring ilmenite ($FeTiO_3$) shows a similar inward diffusion pattern for lattice oxygen in the bulk. Day and Frisch [8] used chromium chromate as an inert marker to study the copper (Cu) oxidation process and found that the diffusion mechanism is the outward diffusion of Cu ions. In general, the dominating diffusing species during the oxidation of oxygen carriers are metal cations. Once the ionic diffusion mode of a volume-expansion or volume-constant reaction is determined, the morphological evolution induced by oxidation can be deduced. The molar volumes for typical oxygen carrier materials are listed in Table 1. The oxidation reaction involving outward ionic diffusion often smoothens concave structures on the particle surfaces [9]. On the other hand, the convex surface is smoothened via a lower outward diffusion flux in the vertical direction. Ionic diffusion in the solid phase with molar volume changes can affect the available surface area during the oxidation reaction. Similar phenomena have been observed during reduction reactions. Hence, these factors should be considered when investigating the morphological evolution of oxygen carriers during redox reactions.

The morphological evolution of oxygen carriers, induced by solid-state ionic diffusion, was also studied on the microscopic level. Qin et al. [10] investigated the oxidation of Fe particles in randomly distributed pores with no visible grain boundaries and found that oxidation at 700 °C results in a mean volume expansion of about 25% and the formation of a porous center arising from the outward diffusion of the Fe ions and inward diffusion of the O ions. Because the outward diffusivity of Fe ions is higher than the inward diffusivity of O ions, there is net Fe transport from the core of the Fe particle to the particle surface, where Fe_2O_3 forms. This outward diffusion of Fe ions is further improved because the volume expansion of Fe particle during oxidation creates more physical space for Fe ion transport. The diffusion also is accompanied by the formations of nanowires and nanopores due to the curvature-driven grain growth (Fig. 2) [10].

However, for the bimetallic oxygen carrier Fe–Ti binary system, the morphological evolution is different than that of the Fe microparticle due to the different diffusion behavior of the titanium (Ti) ion and the Fe ion. At an oxidation temperature of 700 °C, Fe and Ti are oxidized to $FeTiO_3$ with the formation of nanobelts [11]. These nanobelts, which have widths of 150–200 nm and width-to-thickness ratios of 5–10, protrude from the surface of the $FeTiO_3$ oxygen carrier and mainly contain Fe and O [12–14]. Compared with Fe_2O_3 microparticles, $FeTiO_3$ microparticles not only exhibit higher porosity after multiple redox cycles, but also show higher stability which has been confirmed through the reactivity study of over 1000 redox cycles [15]. It indicates that the addition of Ti support can enhance the reactivity and recyclability of iron based oxygen carriers.

Table 1
Molar volume information for typical oxygen carrier materials at different oxidation states.

Metal/metal oxide	Molar volume ($cm^3 \cdot mol^{-1}$)
Fe	7.10
FeO	12.50
Fe_2O_3	30.50
Fe_3O_4	44.70
Fe_2TiO_5	54.40
$FeTiO_3$	31.70
$FeTi_2O_5$	55.30
Fe_2TiO_4	46.00
Co	6.60
CoO	11.60
Co_2O_3	32.00
Co_3O_4	39.40
Ni	6.60
NiO	10.90
Cu	7.10
Cu_2O	23.70
CuO	12.60
Mn	7.60
MnO	13.00
Mn_2O_3	35.11
Mn_3O_4	47.08
MnO_2	17.30

Molar volume reported in the literature varies from study to study, based on different experimental and theoretical methods.

The application of density functional theory (DFT) calculations to study the ionic diffusion of oxygen carriers during chemical looping processes began in the late 2000s [13,16]. The methodology is to create possible interstitial sites for the ions of interest to diffuse through based on ground state energy searching, then to identify the most favorable diffusion pathways by energy barrier calculations. Recently, the diffusion paths of the Fe and Ti ions in oxygen carrier $FeTiO_3$ were investigated by combining first-principles microkinetics and *ab initio* thermodynamics. It was found that the diffusion barrier of Fe ions was much lower than that of Ti ions. Therefore, the outward diffusion of Fe ions is more favorable than that of Ti ions, which explains the formation of Fe_2O_3 nanobelts during the oxidation process [11].

3. Oxygen vacancy of oxygen carriers

During reduction in chemical looping processes, the oxygen carrier donates lattice O atoms for the full oxidation, partial oxidation, or selective oxidation of carbonaceous fuels, leading to the formation of oxygen vacancies. Oxygen vacancies in the bulk or on the surface of metal oxide oxygen carriers may greatly affect their morphology, electronic structure, and chemical properties. An efficient oxygen carrier should allow for sufficient transportation of lattice O atoms from the bulk toward the surface. Thus, an effective oxygen carrier needs to have appropriate oxygen vacancy formation energy so that the required amount of lattice O atoms can release for the oxidation of carbonaceous fuels. Due to the limit of spectroscopic techniques, many computational studies on oxygen vacancies of metal oxides have been performed.

Ceria (CeO_2) has a fluorite structure, which is favorable for the diffusion of lattice O atoms and oxygen vacancy formation. Yang et al. [17] investigated the structural modifications induced by the oxygen vacancy formation on CeO_2 using the spin-polarized PW91 functional, and found that the structural modifications followed a pattern in which cerium (Ce) atoms near to vacancy sites migrated away from the defect sites, while the next-nearest vacancy sites of the lattice O atoms contracted in the region. Vanadium oxide (V_2O_5), which was considered to be most effective oxygen carrier for the selective oxidation of CH_4 to formaldehyde (HCHO), was widely studied recently [18]. Sauer and Dobler [19] investigated the oxygen vacancies on V_2O_5 surface using the 2L cluster model and the B3LYP functional, and reported an oxygen vacancy formation energy of 1.17 eV. This indicated that the lattice O atoms on V_2O_5 surface are easy to release due to the low oxygen vacancy formation energy. In addition to ceria and vanadium oxide, iron oxide is an important oxygen carrier for CH_4 CLR, in which it converts CH_4 to syngas via partial oxidation. In this process, the adsorbed CH_x radicals on the surface bind to lattice O atoms transferred from the bulk of the iron oxide, resulting in the formation of oxygen vacancies. The CH_4 partial oxidation reaction on the iron oxide oxygen carrier is a complex process due to the stepwise reduction: $Fe_2O_3 \rightarrow Fe_3O_4 \rightarrow FeO \rightarrow Fe$. Fan et al. [20,21] investigated the characteristics of the multiple oxidation states of iron, and developed a countercurrent moving bed reactor

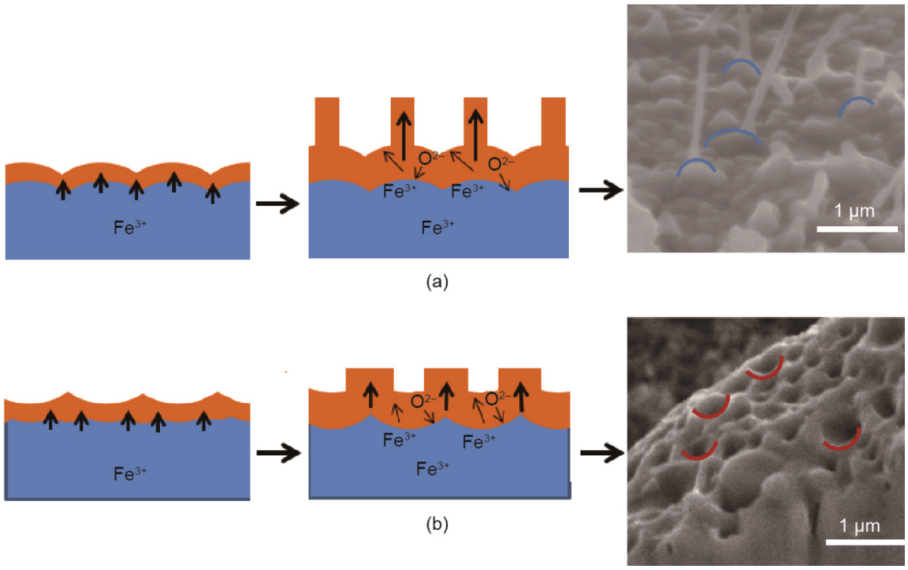

Fig. 2. Formations of (a) Fe_2O_3 nanowires and (b) nanopores. (Reproduced from Ref. [10] with permission from the Royal Society of Chemistry)

system for their application in chemical looping system. Fe_2O_3, Fe_3O_4, and FeO have similar close-packed oxygen structures, thus the redox transitions between each phase are faster than that between FeO and Fe [22,23]. Cheng et al. [24] studied oxygen vacancies in these oxidation phases using the atomistic thermodynamics appraoch and DFT calculations, and found that the formation energies of oxygen vacancies on the surface are lower than that of oxygen vacancies in the subsurface (Table 2 and Fig. 3), which significantly affects the phase transition of iron oxide oxygen carriers.

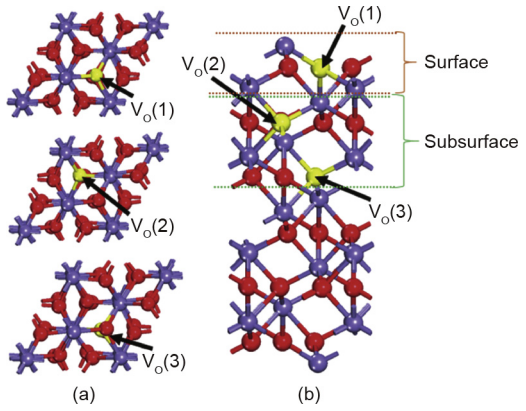

Fig. 3. (a) Top view and (b) sider view of α-Fe_2O_3(001) surface model with oxygen vacancies on the surface and in the subsurface. Purple balls denote Fe atoms, red balls denote lattice O atoms, and yellow balls denote oxygen vacancies. (Reproduced from Ref. [24] with permission from the PCCP Owner Societies)

Without oxygen vacancies, the oxidation process will result in the formation of an iron oxide product layer outside of the original surface, since the diffusion energy barrier for the inward diffusion of O ions is larger than the barrier for the outward diffusion of Fe ions. However, with oxygen vacancies, the diffusion barrier for the inward diffusion of O ions is lower than the barrier for the outward diffusion of Fe ions; thus, the formation of the iron oxide product layer occurs at the Fe_2O_3–Fe interface (Fig. 4).

Cheng et al. [24] also found that TiO_2 support can decrease the formation energy of oxygen vacancies in the iron oxide, thus facilitating oxygen vacancy formation and the transportation of lattice O atoms [11]. Therefore, oxygen vacancy formation in the $FeTiO_3$ phase during reduction is substantially easier than in Fe_2O_3, which explains the superior recyclability of Fe–Ti binary oxygen carrier particles over iron oxide oxygen carrier particles [25].

4. Surface reaction on oxygen carriers

As discussed in the previous sections, the oxygen carriers donate lattice O atoms for the conversion of carbonaceous fuels in chemical looping processes. However, the conversion may proceed via full oxidation, partial oxidation, or selective oxidation. Therefore, a comprehensive understanding on chemical looping redox reaction mechanism is extremely important.

Syngas is a crucial intermediate resource for production of ammonia, methanol, and synthetic hydrocarbon fuels and commonly produced from the partial oxidation of carbonaceous fuels such as methane [26]. A great number of oxygen carriers have been studied for chemical looping partial oxidation applications, including the transition metal oxides of manganese (Mn), Fe, cobalt (Co),

Table 2
Formation energy of oxygen vacancies $V_O(1)$, $V_O(2)$, and $V_O(3)$ in α-Fe_2O_3(001) surface [24].

Oxygen vacancy	E_f (kJ·mol^{-1})	d_{min} (Å)	d_{max} (Å)	Relative probability at 700 °C (%)	Relative probability at 900 °C (%)
$V_O(1)$	258.56	2.03	2.03	100	100
$V_O(2)$	292.51	1.93	2.09	1.51	3.07
$V_O(3)$	342.43	1.91	2.13	3.13×10^{-5}	1.84×10^{-4}

E_f: formation energy; d_{min}: the minimal length of Fe–O bonds; d_{max}: the maximal length of Fe–O bonds.

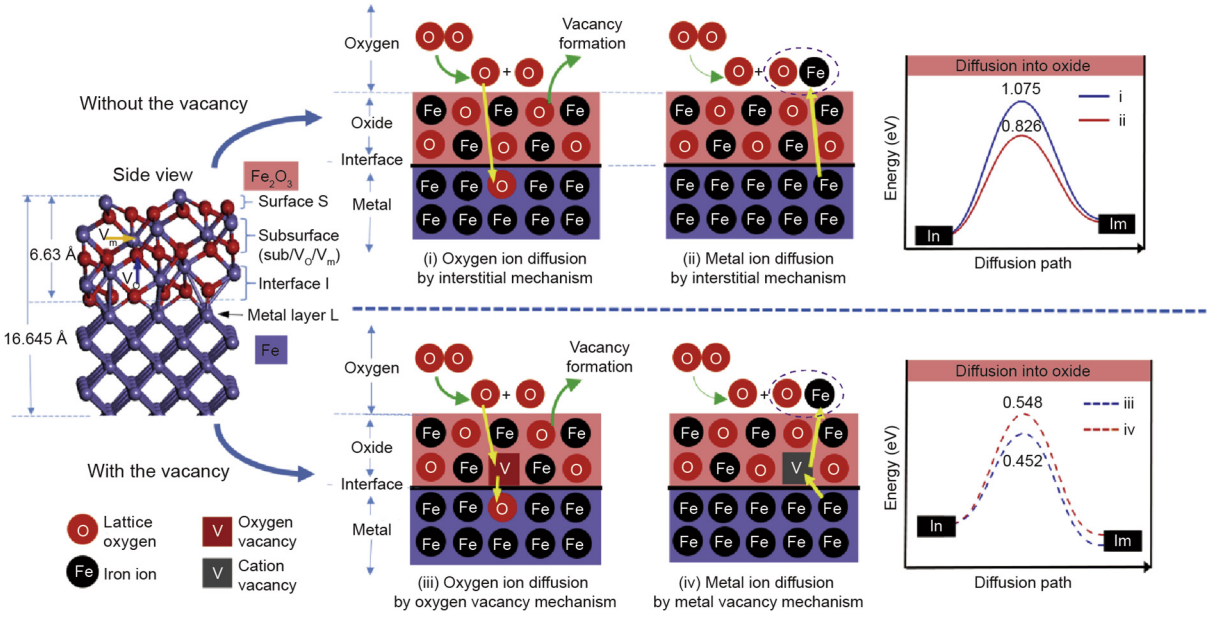

Fig. 4. Oxygen vacancy effect on the ionic diffusion mechanism with diffusion activation energies obtained from DFT calculations. V_O and V_m represent the oxygen vacancy and metal cation vacancy, respectively; In and Im represent the initial state and the intermediate state, respectively.

nickel (Ni), and Cu [25,27–29]. Iron oxide has been widely studied and applied as chemical looping oxygen carrier because it possesses high oxygen capacity meanwhile it is a low-cost environmentally-friendly material. In addition, using iron oxide oxygen carrier, the syngas selectivity can reach over 90% by chemical looping partial oxidation of methane [30]. Jin et al. [31] studied the reduction of iron oxide with methane under different reaction conditions using thermogravimetric analysis/mass spectrometry (TGA-MS), and found that the ventilation air is unfavorable for the release of lattice O atoms. Recently, Cheng et al. [32] investigated the role of oxygen vacancies of iron oxide on chemical looping partial oxidation of methane using DFT + *U* calculations and TGA. They found that O ions in the subsurface prefer to diffuse outward into the vacancy sites on the surface. More importantly, they found that oxygen vacancies can facilitate methane partial oxidation by reducing the activation barrier of the C–H bond in CH_x radicals. The proposed mechanism for the complete and partial oxidation of methane is shown in Fig. 5 [33]. As the figure shows, carbon dioxide (CO_2) and water (H_2O) molecules form during the initial stage of methane oxidation because CH_4 molecules prefer to adsorb on surface Fe sites and then proceed via a complete oxidation pathway when the oxygen vacancy concentration is very low. Monazam et al. [33] applied TGA to investigate methane oxidation on Fe_2O_3 over the range of 700–825 °C, and demonstrated that most of the CH_4 molecules were completely oxidized to CO_2 and H_2O in the early stage of the reduction period; CO and H_2 molecules were then generated via the partial oxidization pathway. This finding was in good agreement with the proposed mechanism depicted in Fig. 5.

Oxygen carrier materials for the oxidative coupling of methane (OCM) have also been extensively studied for their physiochemical properties, especially in terms of structural defects such as oxygen vacancies. The oxygen vacancies of OCM oxygen carrier materials play a vital role in facilitating methane activation from charged oxygen species [34]. Studies have shown that there is a correlation between electrical conductivity and C_2 yields. OCM oxygen carriers with p-type and O ion conductivity within the band gap of 5–6 eV are reported to be the best-performing OCM materials [35]. In addition, methane conversion and C_2 selectivity are important factors for the selection of OCM materials. Many types of oxides have been tested as OCM oxygen carriers, including but not limited to lead(II) oxide (PbO), tin dioxide (SnO_2), gallium(III) oxide (Ga_2O_3), germanium dioxide (GeO_2), indium(III) oxide (In_2O_3), zinc oxide (ZnO), cadmium oxide (CdO), calcium oxide (CaO), magnesium oxide (MgO), and aluminum oxide (Al_2O_3) (Table 3) [36]. A general conclusion obtained from the material screening is that rare earth metal oxides, particularly the lanthanide oxides, tend to have high C_2 selectivity (> 70%), whereas the acidic oxides, including Al_2O_3 and ZSM-5, have low C_2 selectivity [37,38].

The general reaction mechanism for the chemical looping OCM is shown below.

Oxygen carrier reduction:

$$nCH_4 + MO_{z+y} \rightarrow C_nH_{4n-2y} + yH_2O + MO_z$$

Oxygen carrier oxidation:

$$MO_z + (y/2)O_2 \rightarrow MO_{z+y}$$

Although a great deal of ambiguity remains regarding the OCM mechanism that determines the OCM yield and selectivity due to the complicated OCM reaction network [39,40], researchers keep trying to develop efficient approaches for understanding the OCM process and improving the reactivity. Huang et al. [41] proposed a hybrid genetic algorithm to design the OCM materials. Based on the multi-turn design strategy with global optimization, they designed a multi-component OCM catalyst which can achieve C_2 hydrocarbon yield of greater than 25%. Chua et al. [42]

Table 3
Performance of OCM oxygen carriers [36].

OCM oxygen carrier	CH_4/O_2 mole ratio	Temperature (°C)	Methane feed rate ($mol \cdot g_{cat}^{-1} \cdot h^{-1}$)	Specific activity ($\times 10^4$ $mol \cdot m^{-2} \cdot h^{-1}$)						Total C[a]
				H_2	CO_2	CO	C_2H_4	C_2H_6	Total C_2	
5% Li/MgO	3.0	710	0.0616[a]	7.7	16.1	1.3	2.50	8.00	10.50	38.4
MgO	3.0	710	0.0616[a]	3.7	4.5	1.3	0.80	0.80	1.60	9.0
5% Li/La_2O_3	3.0	710	0.0616[a]	20.0	24.0	5.1	1.80	8.90	10.70	50.5
La_2O_3	3.0	710	0.0616[a]	11.0	17.0	1.8	4.20	4.90	9.10	37.0
5% Li/Sm_2O_3	3.0	710	0.0616[a]	16.0	97.0	3.9	29.00	42.00	71.00	242.9
Sm_2O_3	3.0	710	0.0616[a]	19.0	28.0	3.5	5.00	6.80	11.80	55.1
MgO	2.1	700	0.0148	–	–	–	0.02	0.06	0.08	1.4
7% Li/MgO	2.1	700	0.0185	–	–	–	3.00	3.00	6.00	16.5
20% Na/MgO	2.1	700	0.0185	–	–	–	0.21	0.43	0.64	4.2
30% K/MgO	2.1	700	0.0185	–	–	–	0	0.02	0.02	3.0
CaO	2.1	700	0.0185	–	–	–	0.05	0.54	0.59	7.9
5% Li/CaO	2.1	700	0.0185	–	–	–	2.80	3.90	6.70	16.7
15% Na/CaO	2.1	700	0.0185	–	–	–	4.90	5.50	10.40	30.8
23% K/CaO	2.1	700	0.0185	–	–	–	3.50	4.90	8.40	28.7
Y_2O_3	46.0	700	0.0122	–	–	–	0.20	0.46	0.66	1.7
La_2O_3	46.0	700	0.0122	–	–	–	0.15	0.28	0.43	1.0
Sm_2O_3	46.0	700	0.0122	–	–	–	1.10	2.30	3.40	7.3
Gd_2O_3	46.0	700	0.0122	–	–	–	0.37	0.83	1.20	3.0
Ho_2O_3	46.0	700	0.0122	–	–	–	0.24	1.16	1.40	3.3
Yb_2O_3	46.0	700	0.0122	–	–	–	0.10	0.50	0.60	11.4
PbO	46.0	700	0.0122	–	–	–	0.20	2.30	2.50	–
Bi_2O_3	46.0	700	0.0122	–	–	–	0.30	1.60	1.90	5.1
$LaAlO_3$	1.0	710	0.1790[a]	–	–	–	–	–	43.10	178.0
La_2O_3	1.0	710	0.1790[a]	–	–	–	–	–	8.70	37.8
Sm_2O_3	1.0	710	0.1790[a]	–	–	–	–	–	22.50	120.0
CeO_2	2.0	750	0.0298	–	–	–	1.50	0.20	1.70	26.8
Yb_2O_3	2.0	750	0.0298	–	–	–	2.20	2.20	4.40	19.7
$Ce_{0.95}Yb_{0.1}O_{1.95}$	2.0	750	0.0298	–	–	–	0	0.20	0.20	83.4
SrO	2.0	750	0.0298	–	–	–	5.60	2.00	7.60	24.4
$SrCeO_3$	2.0	750	0.0298	–	–	–	12.50	14.70	27.20	110.0
$SrCe_{0.9}Yb_{0.1}O_{2.95}$	2.0	750	0.0298	–	–	–	20.20	13.40	33.60	112.0

[a] Based on methane converted into carbon-containing product.

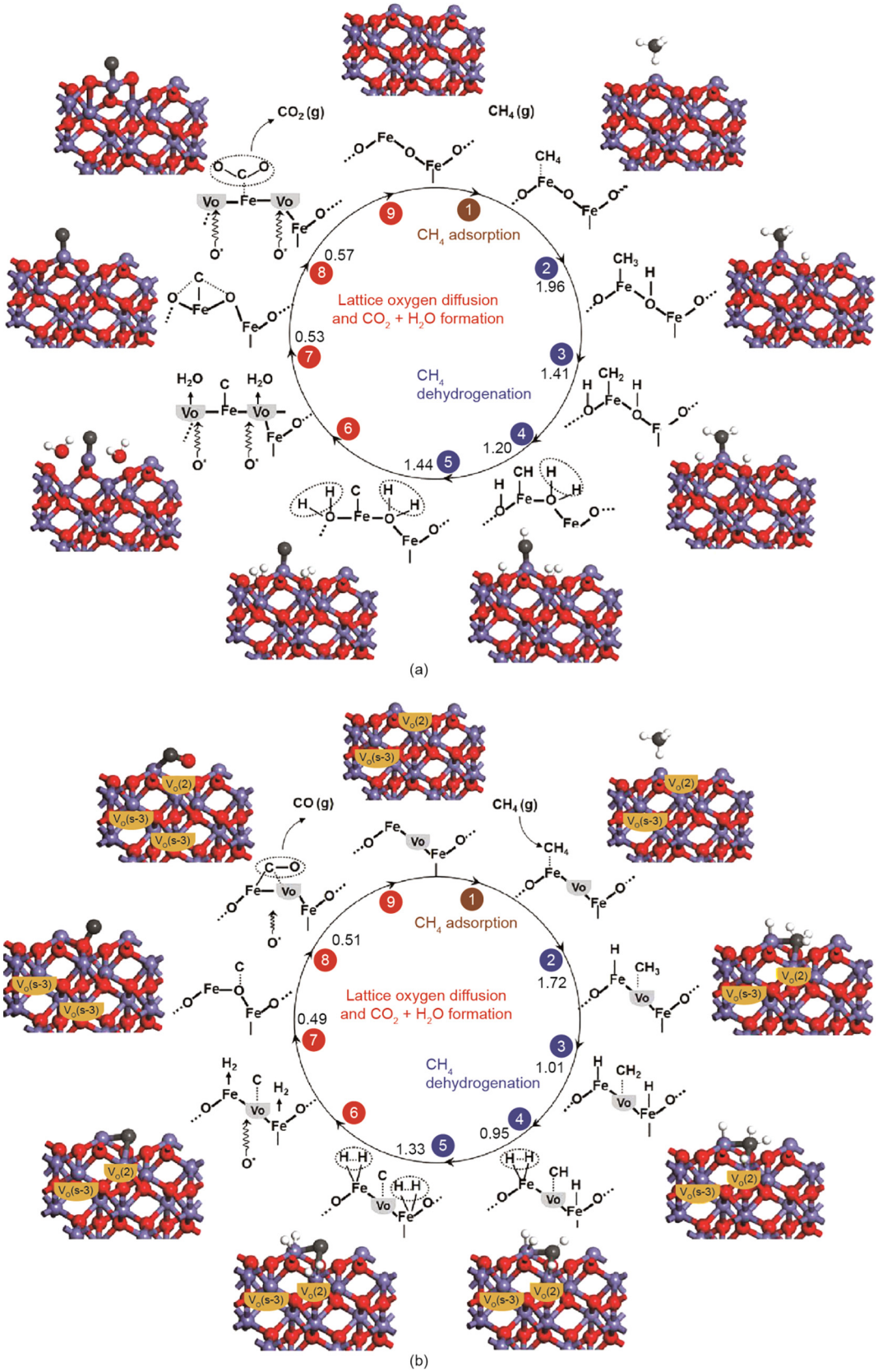

Fig. 5. (a) Complete oxidation and (b) partial oxidation mechanism of methane on iron oxide oxygen carriers. The activation barrier for each elementary step is given in eV units. V_O(s-3) represents the oxygen vacancy in the subsurface, V_O(2) represents the oxygen vacancies on the surface, and O* represents the lattice oxygen which migrates into the oxygen vacancy. (Reproduced from Ref. [33] with permission from the PCCP Owner Societies)

developed a sodium-tungsten-manganese-supported-silica catalyst (Na-W-Mn/SiO_2) and found both Na_2WO_4 and Mn_2O_3 crystalline phases contributed to achieving high selectivity of C_2 products by exploring the interaction effects of the component–component and component–support on the methane conversion and C_{2+} yield. In general, current OCM materials can achieve a C_2 selectivity of 50%–70% and methane conversion of 35%–55% [43]. The continuing studies on the chemical looping technology will facilitate the development of OCM oxygen carriers for achieving higher selectivity and yield.

5. Reactivity improvement of oxygen carriers

Since surface chemistry plays a key role in chemical looping redox processes, extensive efforts have been devoted to catalytically modifying the surface of oxygen carriers for reactivity enhancement [44–46]. Liu and Zachariah [47] synthesized alkali-metal-doped Fe_2O_3/Al_2O_3 oxygen carriers and found alkali metal doping (~5 mol%) with Na, K, and Cs can stabilize the reactivity of the Fe_2O_3 more than 50 redox cycles. Wang et al. [48] investigated a series of Zr-doped Cu-based oxygen carriers, and demonstrated that the Zr-doping amount can improve the oxygen-release capacity. Mohamed et al. [49] studied the effect of Ce dopant on a NiO/Ce-γAl_2O_3 oxygen carrier and reported that NiO with 2%–10% Ce can greatly enhance CO conversion. Chen et al. [50] recently demonstrated that tungsten-based oxygen carriers with nickel modification were effective for the chemical looping partial oxidation of methane. Their results indicated that the oxygen availability, methane conversion, and syngas yield can be significantly increased over $Ni_{0.5}WO_x/Al_2O_3$ compared with WO_3/Al_2O_3. Qin et al. [51] recently initiated a work on low-concentration dopant modification over oxygen carrier for reactivity improvement. They used isovalent lanthana (La) dopants at a very low concentration relative to the total concentration of iron

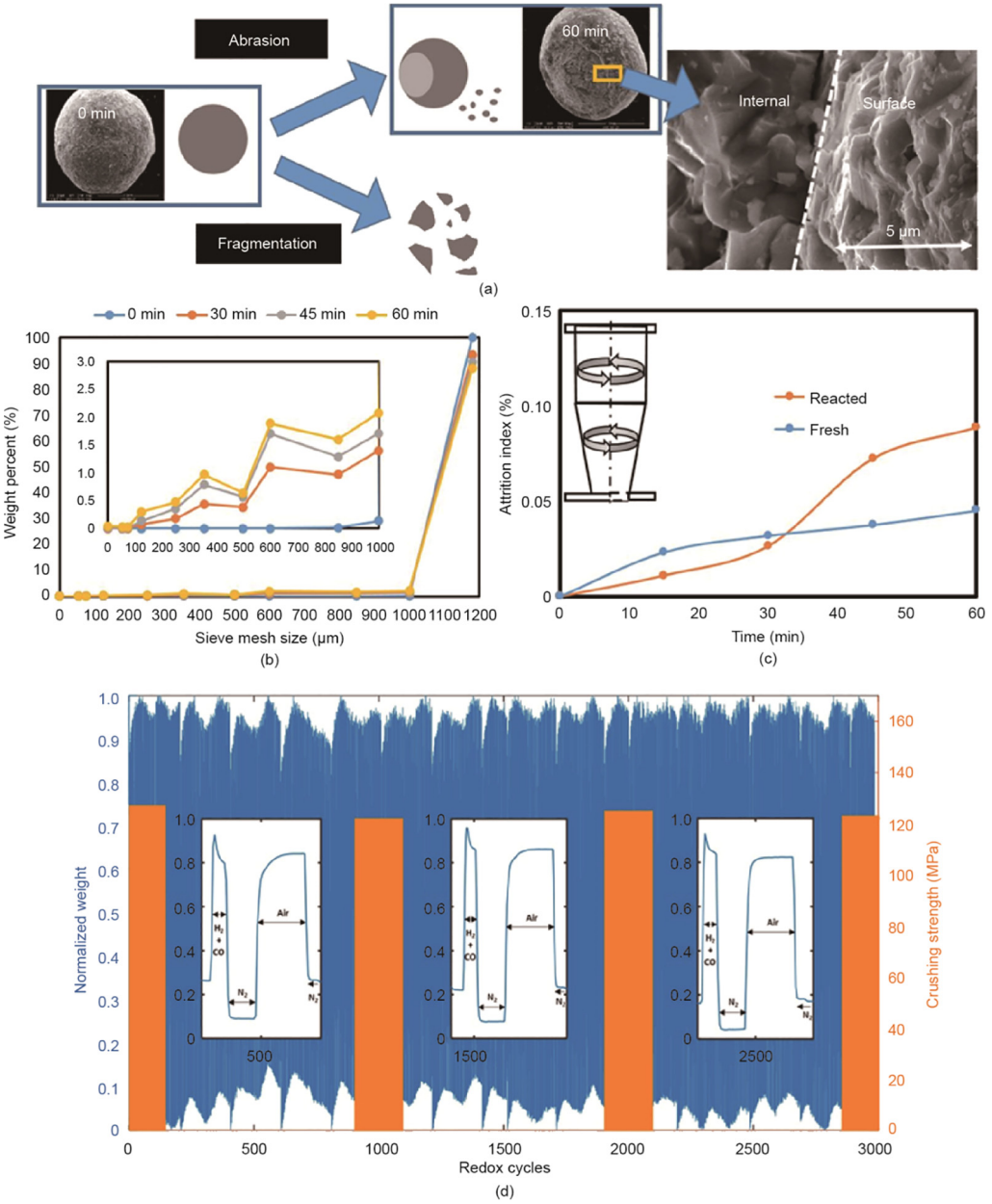

Fig. 6. (a) Mechanism of attrition with SEM images of fresh (0 min) and eroded oxygen carrier (60 min) after jet-cup; (b) evolution in particle size distribution in a jet-cup experiment; (c) comparison of attrition index between fresh and reacted composite oxygen carrier from pilot operation; (d) normalized real-time TGA data over 3000 redox cycles with crushing strength measurements. (Reproduced from Ref. [52] with permission from the EES Owner Societies)

oxide oxygen carriers (e.g., < 1%) so that the oxygen carrier can keep high oxygen capacity without phase change. They found 1% of La dopant leads to a 178% increase in reduction reactivity and a 156% increase in re-oxidation reactivity for CH_4 gasification reactions, compared with updoped iron oxide. It is because La dopant significantly lowers the barrier of C–H bond (CH_4 and CH_x radicals) activation during oxygen carrier reduction. Recently, Chung et al. [52] reported an iron-based composite oxygen carrier with an Al-based skeleton which exhibits high reactivity and recyclability over 3000 TGA redox cycles at 1000 °C. This oxygen carrier also was tested extensively in both pilot and sub-pilot scale reactors exhibiting low attrition rates as shown in Fig. 6 [52]. These findings provide a strategy for designing highly active oxygen carrier using a relatively simple fabrication process.

In chemical looping partial oxidation processes, methane oxidation occurs in the reducer, which is typically either a fluidized bed or a moving bed. The fluidized bed has excellent heat-transfer characteristics, but it is difficult to maintain a uniformly desired oxidation state of the metal oxide oxygen carrier for methane oxidation due to a wide distribution of the residence time in a fluidized bed. The moving bed can achieve high CH_4 conversion (> 99.9%) with a syngas purity of 91% at the sub-pilot scale [26]. In addition, it can maintain a high oxygen carrier conversion and hence a low oxygen carrier circulation rate in the reactor. However, there are still challenges to be overcome in industrial applications, such as stabilizing the continuous long operation of the chemical looping process, controlling the proper heat balance between the oxidizer and reducer, and maintaining the recyclability properties of the oxygen carriers. Therefore, an appropriate design for an oxidizer and reducer to treat solid feed materials during the sustained redox reactions of reactive oxygen carriers under high temperature and pressure will also be a focus of studies on chemical looping technology development.

6. Summary

The oxygen carrier materials in chemical looping play a crucial role in achieving high efficiency compared with conventional fuel-conversion processes. Metal oxide oxygen carriers are required to have high reactivity and recyclability while undergoing cyclic redox reactions with lattice oxygen transport at high chemical looping temperatures. Therefore, it is essential to fully understand the effects of the various chemical and physical characteristics of the crystal phases on the ionic diffusion process, with particular focus on the diffusion energy barrier, oxygen vacancy formation energy, and surface reaction mechanism. Understanding the mechanism can both provide theoretical guidance on fabricating active oxygen carrier materials and predict the performance of particles with minimum trial-and-error screening. It is noted that earlier experimental marker and isotope studies that confirmed the ionic diffusion mechanism for the sulfation reaction [53,54] of CaO and SO_2 provide a fundamental framework for the current analyses of the redox reactions of the metal oxides involved in chemical looping systems. The recyclability of metal oxide oxygen carriers can be promoted by adding supportive oxides that lower the oxygen vacancy energy and increase the lattice oxygen diffusivity. On the other hand, dopant modification can significantly improve the surface reactivity of metal oxide oxygen carriers, such as iron-oxide-based oxygen carriers. These findings provide new insight into the factors affecting the properties of oxygen carriers during chemical looping redox processes. It should be noted that a combined experimental and computational approach will facilitate the development of metal oxide oxygen carriers with improved ionic diffusion, reactivity, selectivity, and structural stability.

Compliance with ethics guidelines

Zhuo Cheng, Lang Qin, Jonathan A. Fan, and Liang-Shih Fan declare that they have no conflict of interest or financial conflicts to disclose.

References

[1] Qin L, Guo M, Cheng Z, Xu M, Liu Y, Xu D, et al. Improved cyclic redox reactivity of lanthanum modified iron-based oxygen carriers in carbon monoxide chemical looping combustion. J Mater Chem A 2017;5(38):20153–60.
[2] Mattisson T, Lyngfelt A, Leion H. Chemical-looping with oxygen uncoupling for combustion of solid fuels. Int J Greenh Gas Control 2009;3(1):11–9.
[3] Hallberg P, Källén M, Jing D, Snijkers F, van Noyen J, Rydén M, et al. Experimental investigation of based oxygen carriers used in continuous chemical-looping combustion. Int J Chem Eng 2014;2014:1–9.
[4] Bakken E, Norby T, Stølen S. Nonstoichiometry and reductive decomposition of $CaMnO_{3-\delta}$. Solid State Ion 2005;176(1–2):217–23.
[5] Gu H, Shen L, Xiao J, Zhang S, Song T. Chemical looping combustion of biomass/coal with natural iron ore as oxygen carrier in a continuous reactor. Energy Fuels 2011;25(1):446–55.
[6] Li F, Kim HR, Sridhar D, Wang F, Zeng L, Chen J, et al. Syngas chemical looping gasification process: oxygen carrier particle selection and performance. Energy Fuels 2009;23(8):4182–9.
[7] Li F, Sun Z, Luo S, Fan LS. Ionic diffusion in the oxidation of iron—effect of support and its implications to chemical looping applications. Energy Environ Sci 2011;4(3):876–80.
[8] Day RJ, Frisch MA. Chromium chromate as an inert marker in copper oxidation. Surf Interface Anal 1986;8(1):33–6.
[9] Chiang YM, Birnie DP, Kingery WD. Physical ceramics: principles for ceramic science and engineering. New York: John Wiley & Sons; 1996.
[10] Qin L, Majumder A, Fan JA, Kopechek D, Fan LS. Evolution of nanoscale morphology in single and binary metal oxide microparticles during reduction and oxidation processes. J Mater Chem A 2014;2(41):17511–20.
[11] Qin L, Cheng Z, Fan JA, Kopechek D, Xu D, Deshpande N, et al. Nanostructure formation mechanism and ion diffusion in iron–titanium composite materials with chemical looping redox reactions. J Mater Chem A 2015;3(21):11302–12.
[12] Fu Y, Chen J, Zhang H. Synthesis of Fe_2O_3 nanowires by oxidation of iron. Chem Phys Lett 2001;350(5–6):491–4.
[13] Wen X, Wang S, Ding Y, Wang ZL, Yang S. Controlled growth of large-area, uniform, vertically aligned arrays of α-Fe_2O_3 nanobelts and nanowires. J Phys Chem B 2005;109(1):215–20.
[14] Dang HY, Wang J, Fan SS. The synthesis of metal oxide nanowires by directly heating metal samples in appropriate oxygen atmospheres. Nanotechnology 2003;14(7):738–41.
[15] Fan LS. Chemical looping systems for fossil energy conversions. Hoboken: John Wiley & Sons; 2010.
[16] Wilson NC, Muscat J, Mkhonto D, Ngoepe PE, Harrison NM. Structure and properties of ilmenite from first principles. Phys Rev B 2005;71(7):075202.
[17] Yang Z, Woo TK, Baudin M, Hermansson K. Atomic and electronic structure of unreduced and reduced CeO_2 surfaces: a first-principles study. J Chem Phys 2004;120(16):7741–9.
[18] Chen L, Lu Y, Hong Q, Lin J, Dautzenberg FM. Catalytic partial oxidation of methane to syngas over Ca-decorated-Al_2O_3-supported Ni and NiB catalysts. Appl Catal A Gen 2005;292:295–304.
[19] Sauer J, Dobler J. Structure and reactivity of V_2O_5: bulk solid, nanosized clusters, species supported on silica and alumina, cluster cations and anions. Dalton Trans 2004;19(19):3116–21.
[20] Thomas TJ, Fan LS, Gupta P, Velazquez-Vargas LG, inventors; The Ohio State University, assignee. Combustion looping using composite oxygen carriers. United States patent US 7767191. 2010 Aug 3.
[21] Tong A, Zeng L, Kathe MV, Sridhar D, Fan LS. Application of the moving-bed chemical looping process for high methane conversion. Energy Fuels 2013;27(8):4119–28.
[22] Pineau A, Kanari N, Gaballah I. Kinetics of reduction of iron oxides by H_2: Part I: low temperature reduction of hematite. Thermochim Acta 2006;447(1):89–100.
[23] Pineau A, Kanari N, Gaballah I. Kinetics of reduction of iron oxides by H_2: Part II: low temperature reduction of magnetite. Thermochim Acta 2007;456(2):75–88.
[24] Cheng Z, Qin L, Guo M, Fan JA, Xu D, Fan LS. Methane adsorption and dissociation on iron oxide oxygen carriers: the role of oxygen vacancies. Phys Chem Chem Phys 2016;18(24):16423–35.
[25] De Diego LF, Ortiz M, Adánez J, García-Labiano F, Abad A, Gayán P. Synthesis gas generation by chemical-looping reforming in a batch fluidized bed reactor using Ni-based oxygen carriers. Chem Eng J 2008;144(2):289–98.
[26] Fan LS. Chemical looping partial oxidation: gasification, reforming, and chemical syntheses. Cambridge: Cambridge University Press; 2017.
[27] He F, Wei Y, Li H, Wang H. Synthesis gas generation by chemical-looping reforming using Ce-based oxygen carriers modified with Fe, Cu, and Mn oxides. Energy Fuels 2009;23(4):2095–102.

[28] Azimi G, Mattisson T, Leion H, Rydén M, Lyngfelt A. Comprehensive study of Mn–Fe–Al oxygen-carriers for chemical-looping with oxygen uncoupling (CLOU). Int J Greenh Gas Control 2015;34:12–24.
[29] Qin L, Cheng Z, Guo M, Fan JA, Fan LS. Morphology evolution and nanostructure of chemical looping transition metal oxide materials upon redox processes. Acta Mater 2017;124:568–78.
[30] Luo S, Zeng L, Xu D, Kathe M, Chung E, Deshpande N, et al. Shale gas-to-syngas chemical looping process for stable shale gas conversion to high purity syngas with a H_2:CO ratio of 2:1. Energy Environ Sci 2014;7(12):4104–17.
[31] Jin Y, Sun C, Su S. Experimental and theoretical study of the oxidation of ventilation air methane over Fe_2O_3 and CuO. Phys Chem Chem Phys 2015;17(25):16277–84.
[32] Cheng Z, Qin L, Guo M, Xu M, Fan JA, Fan LS. Oxygen vacancy promoted methane partial oxidation over iron oxide oxygen carriers in the chemical looping process. Phys Chem Chem Phys 2016;18(47):32418–28.
[33] Monazam ER, Breault RW, Siriwardane R, Richards G, Carpenter S. Kinetics of the reduction of hematite (Fe_2O_3) by methane (CH_4) during chemical looping combustion: a global mechanism. Chem Eng J 2013;232:478–87.
[34] Liu S, Tan X, Li K, Hughes R. Methane coupling using catalytic membrane reactors. Catal Rev 2001;43(1–2):147–98.
[35] Malekzadeh A, Khodadadi A, Abedini M, Amini M, Bahramian A, Dalai AK. Correlation of electrical properties and performance of OCM $MO_x/Na_2WO_4/SiO_2$ catalysts. Catal Commun 2001;2(8):241–7.
[36] Hutchings GJ, Scurrell MS, Woodhouse JR. Oxidative coupling of methane using oxide catalysts. Chem Soc Rev 1989;18:251–83.
[37] Choudhary VR, Rane VH. Acidity/basicity of rare-earth oxides and their catalytic activity in oxidative coupling of methane to C_2-hydrocarbons. J Catal 1991;130(2):411–2.
[38] Dubois JL, Cameron CJ. Common features of oxidative coupling of methane cofeed catalysts. Appl Catal 1990;67(1):49–71.
[39] Greish AA, Glukhov LM, Finashina ED, Kustov LM, Sung J, Choo K, et al. Oxidative coupling of methane in the redox cyclic mode over the catalysts on the basis of CeO_2 and La_2O_3. Mendeleev Commun 2010;20(1):28–30.
[40] Sung JS, Choo KY, Kim TH, Greish A, Glukhov L, Finashina E, et al. Peculiarities of oxidative coupling of methane in redox cyclic mode over Ag-La_2O_3/SiO_2 catalysts. Appl Catal A Gen 2010;380(1–2):28–32.
[41] Huang K, Zhan XL, Chen FQ, Lü DW. Catalyst design for methane oxidative coupling by using artificial neural network and hybrid genetic algorithm. Chem Eng Sci 2003;58(1):81–7.
[42] Chua YT, Mohamed AR, Bhatia S. Oxidative coupling of methane for the production of ethylene over sodium-tungsten-manganese-supported-silica catalyst (Na-W-Mn/SiO_2). Appl Catal A Gen 2008;343(1–2):142–8.
[43] Sahebdelfar S, Ravanchi MT, Gharibi M, Hamidzadeh M. Rule of 100: an inherent limitation or performance measure in oxidative coupling of methane? J Nat Gas Chem 2012;21(3):308–13.
[44] Cao Y, Sit SP, Pan WP. Preparation and characterization of lanthanum-promoted copper-based oxygen carriers for chemical looping combustion process. Aerosol Air Qual Res 2014;14(2):572–84.
[45] Cao Y, Sit SP, Pan WP. Lanthanum-promoted copper-based oxygen carriers for chemical looping combustion process. J Therm Anal Calorim 2014;116(3):1257–66.
[46] Niu T, Liu GL, Chen Y, Yang J, Wu J, Cao Y, et al. Hydrothermal synthesis of graphene-$LaFeO_3$ composite supported with Cu-Co nanocatalyst for higher alcohol synthesis from syngas. Appl Surf Sci 2016;364:388–99.
[47] Liu L, Zachariah MR. Enhanced performance of alkali metal doped Fe_2O_3 and Fe_2O_3/Al_2O_3 composites as oxygen carrier material in chemical looping combustion. Energy Fuels 2013;27(8):4977–83.
[48] Wang M, Liu J, Hu J, Liu F. O_2–CO_2 mixed gas production using a Zr-doped Cu-based oxygen carrier. Ind Eng Chem Res 2015;54(40):9805–12.
[49] Mohamed SA, Quddus MR, Razzak SA, Hossain MM, de Lasa HI. NiO/Ce-γAl_2O_3 oxygen carrier for chemical looping combustion. Energy Fuels 2015;29(9):6095–103.
[50] Chen S, Zeng L, Tian H, Li X, Gong J. Enhanced lattice oxygen reactivity over Ni-modified WO_3-based redox catalysts for chemical looping partial oxidation of methane. ACS Catal 2017;7(5):3548–59.
[51] Qin L, Cheng Z, Guo M, Fan JA, Fan LS. Impact of 1% lanthanum dopant on carbonaceous fuel redox reactions with an iron-based oxygen carrier in chemical looping processes. ACS Energy Lett 2017;2(1):70–4.
[52] Chung C, Qin L, Shah V, Fan LS. Chemically and physically robust, commercially-viable iron-based composite oxygen carriers sustainable over 3000 redox cycles at high temperatures for chemical looping applications. Energy Environ Sci 2017;10:2318.
[53] Hsia C, St Pierre GR, Raghunathan K, Fan LS. Diffusion through the $CaSO_4$ formed during the reaction of CaO with SO_2 and O_2. AIChE J 1993;39(4):698–700.
[54] Hsia C, St Pierre GR, Fan LS. Isotope study on diffusion in the $CaSO_4$ formed in the sorbent-flue gas reaction. AIChE J 1995;41(10):2337–40.